Dalton Transactions

PAPER

View Article Online
View Journal | View Issue

Cite this: *Dalton Trans.*, 2014, **43**, 10947

Metal ions and solvents ratio co-regulate four new magnetic coordination polymers based upon an unsymmetric tricarboxylate acid ligand†

Yuan-Pu Li, Ying Chai, Guo-Ping Yang, Hui-Hui Miao, Lin Cui, Yao-Yu Wang* and Qi-Zhen Shi

Received 4th April 2014,
Accepted 15th May 2014

DOI: 10.1039/c4dt00995a

www.rsc.org/dalton

Four new coordination polymers (CPs), $[Co_3(L)_2(bib)_3(EtOH)_2]\cdot 2H_2O$ (**1**), $[Mn_3(L)_2(bib)_2(H_2O)_4]\cdot 4H_2O$ (**2**), $[Ni(HL)(bib)(H_2O)_3]$ (**3**) and $[Ni_3(bib)_4(H_2O)_{10}]\cdot 2(L)\cdot 12(H_2O)$ (**4**), were synthesized under solvothermal conditions with an unsymmetrical tricarboxylic acid ligand [biphenyl-3,3′,5-tricarboxylic acid (H_3L)] in the presence of the 1,4-bis(1*H*-imidazol-4-yl)benzene (bib) ligand. In compound **1**, tricarboxylate acid ligands (H_3L) link Co centers to generate two-dimensional (2D) layers which are further connected by bib ligands to exhibit a three-dimensional (3D) framework with a (4,4,5)-connected $(4^2\cdot 6^3\cdot 8)_2(4^2\cdot 6^7\cdot 8)_2(6^4\cdot 8\cdot 10)$ topology. The three-dimensional (3D) framework of **2** is defined as a (3,3,4)-connected topology with the point symbol of $(6\cdot 8^2)_2(6^2\cdot 8)_2(8\cdot 10^4\cdot 12)$. Compound **3** contains a one-dimensional (1D) left-hand helix chain along the *a* direction and further extends into a 2D supramolecular network and a 3D supramolecular framework *via* hydrogen bonds. Compound **4** displays a one-dimensional (1D) molecular ladder, which is further combined with each other through π···π stacking to extend into 2D supramolecular sheets. The supramolecular networks of **3** and **4** resulted from the different solvent ratios [V(H_2O)–V(EtOH)] in the reaction. All the CPs are characterized by single-crystal X-ray diffraction analyses, powder X-ray diffraction (PXRD), elemental analyses, IR spectroscopy, and TGA analyses. Moreover, the weak ferromagnetic properties of **2** and **3** and antiferromagnetic properties of **1** and **4** have also been investigated.

Introduction

The rational design, syntheses and characterization of functional coordination polymers (CPs) have attracted more and more interest not only because of their fascinating structures,[1] but also owing to their tremendous potential applications in gas storage, magnetism, ion exchange, microelectronics, nonlinear optics, and heterogeneous catalysis.[2–4] Generally, there are a variety of factors influencing the topological architectures and properties of the coordination polymers, including the nature of metal ions, organic ligands, solvents, supermolecular forces and so on.[5,6] Undoubtedly, the judicious selection of ligands plays a crucial role in the construction of novel coordination polymers (CPs) owing to their abundant coordination modes to satisfy the geometric requirement of metal centers in constructing fascinating structural architectures.

It is well-known that the symmetric carboxylate ligands have been studied comprehensively, because these types of ligands often directly contribute to the formation of 3D frameworks with high symmetry, exhibiting high surface areas and high pore volumes.[7] In contrast, research on coordination polymers constructed from unsymmetrical tricarboxylate ligands is relatively rare.[8,9] The position of carboxylate groups on the ligands may have an influence on the assembling processes, the structures and even the properties of coordination polymers due to their geometric and electronic effects.[10] Therefore, an unsymmetrical tricarboxylate ligand (H_3L = biphenyl-3,3′,5-tricarboxylic acid) is chosen to construct frameworks with more versatile topologies.[11] This ligand possesses several interesting characteristics: (i) it has three carboxyl groups that may be completely or partially deprotonated, inducing rich coordination modes and interesting topology; (ii) it could act as a hydrogen-bond acceptor as well as a donor, depending upon the degree of deprotonation; (iii) it could conform to the

Key Laboratory of Synthetic and Natural Functional Molecule Chemistry of the Ministry of Education, Shaanxi Key Laboratory of Physico-Inorganic Chemistry, College of Chemistry and Materials Science, Northwest University, Xi'an 710069, P.R. China. E-mail: wyaoyu@nwu.edu.cn; Tel: +86 29 88302604

†Electronic supplementary information (ESI) available: Crystallographic data, fitted curve of emission lifetime, selected bond lengths and angles, PXRD, FTIR, pore size distribution, and the calculation on CO_2 selectivity and enthalpies. CCDC 991512–991515 for compounds **1–4**. For ESI and crystallographic data in CIF or other electronic format see DOI: 10.1039/c4dt00995a

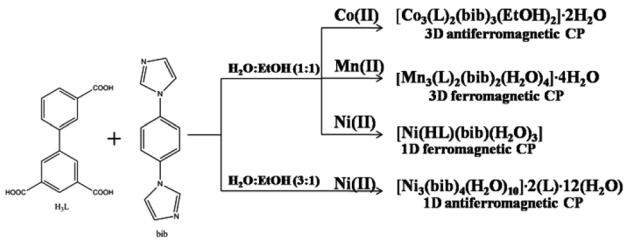

Scheme 1 Synthetic details of compounds **1–4**.

coordination geometries of the metal ions because the three carboxyl groups of H_3L separated by two phenyl rings can form different dihedral angles through the rotation of C–C single bonds leading to new structures.

In this work, we have successfully synthesized four new coordination polymers based on the rigid linear tricarboxylate ligand and the N-donor dipyridyl ligand with three different metal salts under solvothermal conditions (Scheme 1), namely $[Co_3(L)_2(bib)_3(EtOH)_2]\cdot 2H_2O$ (**1**), $[Mn_3(L)_2(bib)_2(H_2O)_4]\cdot 4H_2O$ (**2**), $[Ni(HL)(bib)(H_2O)_3]$ (**3**) and $[Ni_3(bib)_4(H_2O)_{10}]\cdot 2(L)\cdot 12(H_2O)$ (**4**), which feature different architectures respectively. The magnetic properties and thermal stability of the compounds have also been analysed.

Experimental section

Materials and general methods

The solvents and materials were commercially available and used as received. The FT-IR spectra were measured in the range of 4000–400 cm^{-1} on a Bruker EQUINOX-55 spectrometer with KBr pellets. C, H, and N microanalyses were performed using a Vario EL III elemental analyzer (Elementar Analysensysteme GmbH, Germany). The PXRD data were collected on a Bruker D8 ADVANCE with Cu-Kα radiation (λ = 1.5418 Å). Magnetic properties were tested on a Quantum Design MPMS-XL-7 SQUID magnetometer. Thermogravimetric analyses (TGA) were carried out in a nitrogen stream using a NETZSCH STA449C instrument with a heating rate of 10 °C min^{-1}.

Syntheses of $[Co_3(L)_2(bib)_3(EtOH)_2]\cdot 2H_2O$ (1). A mixture of $Co(CH_3COO)_2\cdot 2H_2O$ (12.5 mg, 0.05 mmol), H_3L (14.2 mg, 0.05 mmol) and bib (10.5 mg, 0.05 mmol) was dissolved in a solution of distilled water and EtOH [V(H_2O)–V(EtOH) = 1 : 1]. The solution was added into a Teflon-lined stainless steel vessel (15 mL), heated to 130 °C for 72 h and then cooled to room temperature at a rate of 2 °C h^{-1}. Red block crystals of **1** were obtained (Yield: 45% based on the amount of H_3L). Anal. calcd for $C_{70}H_{54}N_{12}O_{16}Co_3$: C, 56.15; H, 3.83; N, 11.23%. Found: C, 56.09; H, 3.80; N, 11.19%. IR (KBr, cm^{-1}): 3425(s), 3134(m), 3077(w), 2961(w), 2028(m), 1622(m), 1521(s), 1369(s), 1310(w), 1253(m), 1057(s), 967(w), 830(m), 767(m), 720(m), 651(w).

Syntheses of $[Mn_3(L)_2(bib)_3(H_2O)_4]\cdot 2H_2O$ (2). Compound **2** was synthesized in a similar way to that described for **1**, except that $Co(CH_3COO)_2\cdot 2H_2O$ was replaced by $Mn(CH_3COO)_2\cdot 4H_2O$ (12.2 mg, 0.05 mmol). Colorless crystals were obtained (yield: 47%). Anal. calcd for $C_{54}H_{50}N_8O_{20}Mn_3$: C, 53.78; H, 4.15; N, 9.29%. Found: C, 53.69; H, 4.31; N, 9.54%. IR (KBr, cm^{-1}): 3148(s), 2542(w), 1688(vs), 1558(s), 1356(s), 1331(w), 1228(w), 1057(s), 936(m), 889(w), 829(m), 726(w), 678(m), 627(w).

Syntheses of $Ni(HL)(bib)(H_2O)_3$ (3). A mixture of $Ni(CH_3COO)_2\cdot 4H_2O$ (12.5 mg, 0.05 mmol), H_3L (14.2 mg, 0.05 mmol) and bib (10.5 mg, 0.05 mmol) was dissolved in a solution of distilled water and EtOH [V(H_2O)–V(EtOH) = 1 : 1]. The solution was transferred to a Teflon-lined stainless steel vessel (15 mL), heated to 130 °C for 72 h and then cooled to room temperature at a rate of 2 °C h^{-1}. Blue block crystals of **3** were obtained (yield 43%). Anal. calcd for $C_{27}H_{24}N_4O_9Ni$; C, 53.38; H, 3.95; N, 9.23%. Found: C, 53.51; H, 3.89; N, 9.19% IR (KBr cm^{-1}): 3131(s), 2592(w), 1693(vs), 1560(s), 1358(s), 1301(w), 1232(w), 1059(s), 949(m), 897(w), 840(m), 729(w), 690(m), 638(w).

Syntheses of $[Ni_3(bib)_4(H_2O)_{10}]\cdot 2(L)\cdot 12(H_2O)$ (4). Compound **4** was synthesized by a similar procedure used for **3** except that the hydrothermal reaction changes to [V(H_2O)–V(EtOH) = 1 : 1], and blue block crystals of **4** were obtained (yield 53%). Anal. calcd for $C_{78}H_{74}N_{16}O_{34}Ni_3$; C, 47.88; H, 3.78; N, 11.46%. Found: C, 49.01; H, 3.68; N, 11.39% IR (KBr cm^{-1}): 3406(s), 3117(w), 3071(w), 1613(w), 1531(s), 1365(m), 1312(s), 1139(s), 1051(s), 961(m), 920(w), 886(m), 840(s), 764(m), 718(m).

X-ray data collection and structure determination

The diffraction experiments were conducted on a Bruker SMART APEX II CCD detector at 296(2) K using Mo Kα radiation (λ = 0.71073 Å) and ω rotation scans at a width of 0.3°. The structures were solved by the direct methods and refined by the full-matrix least-squares method based on F^2 using SHELX-97.[12] All non-hydrogen atoms were refined anisotropically and hydrogen atoms attached to the C-atom and N-atom were fixed at calculated positions and refined using a riding model. The hydrogen atoms from their parent atoms of ligands were treated as a riding model. Details of data collection and refinement for **1–4** are summarized in Table S1,† and selected bond lengths and angles are listed in Table S2.†

Results and discussion

Crystal structure of $[Co_3(L)_2(bib)_3(EtOH)_2]\cdot 2H_2O$ (1)

X-ray single-crystal diffraction analysis reveals that compound **1** is a complicated 3-nodal (4,4,5)-connected 3D framework. It crystallizes in the triclinic crystal system with the space group of $P\bar{1}$. The asymmetric unit consists of one and a half crystallographically independent Co(II) ions, one completely deprotonated L ligands, one and a half bib ligands, one coordinated ethanol molecule and one water molecule of crystallization. As shown in Fig. 1a, the Co1 is located in a slightly distorted CoN_2O_4 octahedron geometry, completed by two oxygen atoms from two L ligands, two oxygen atoms from two ethanol molecules [Co–O = 2.094(5)–2.119(6) Å], and two nitrogen atoms from two bib ligands [Co–N = 2.149(5) Å]. The bond angles

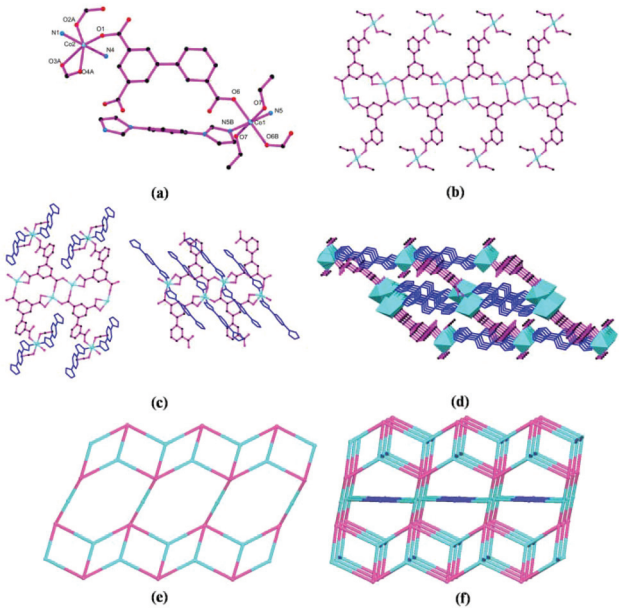

Fig. 1 (a) Coordination environment of Co(II) in compound **1** (black C, red O, blue N, cyan Co); (b) the 2D framework of Co(II) ignoring the connections with bib ligands along the *c* axis; (c) bib ligands coordinated with Co(II) ions in different directions; (d) view of the three-dimensional framework of **1**; (e) schematic representation of the (3,4)-connected layer (blue balls represent the Co atoms, while the purple balls represent the L ligands); (f) perspective view of the (4,4,5)-connected topology for **1** (all hydrogen atoms and lattice water molecules are omitted for clarity). Symmetry codes: (A) $1-x, 2-y, 2-z$; (B) $-x,-y, 1-z$.

around Co1 range from 86.4(2) to 180.0 (1)°. Each Co2 center is surrounded by two nitrogen atoms from two different bib ligands [Co–N = 2.122(6)–2.148(5) Å], and four carboxylic oxygen atoms from three different L ligands [Co–O = 2.070(4)–2.256(5) Å], forming a severely distorted CoN_2O_4 octahedron. The bond angles around Co2 range from 59.92(16) to 177.7(2)°. Three carboxylic groups of each L ligand adopt μ_1–η^1:η^0, μ_1–η^1:η^1 and μ_2–η^1:η^1 coordination modes (Scheme 2a) to bridge adjacent Co(II) ions to form 2D nets (Fig. 1b) and bib ligands coordinated with Co(II) ions in different directions (Fig. 1c) to expand the 2D layers into a 3D coordination network (Fig. 1d). To clearly understand such a complicated architecture, the topological method is used to simplify the structure. For the 2D layers, each Co1 center connects two L ligands, each Co2 center connects three L ligands and each L ligand bridges four metal ions (one Co1 and three Co2), so they can be treated as 3- and 4-connected nodes, respectively; thus the 2D layer is abstracted into a (3,4)-connected network (two-connected Co1 nodes are not shown), as shown in Fig. 1e. Besides, these layers are linked to each other through the connection of bib to bridge Co1 and Co2 ions to form a 3D framework, so the Co1 centers turn into 4-connected nodes and the Co2 centers turn into 5-connected nodes. Accordingly, the whole structure became a charming trinodal (4,4,5)-connected framework with the point symbol of $(4^2{\cdot}6^3{\cdot}8)_2(4^2{\cdot}6^7{\cdot}8)_2(6^4{\cdot}8{\cdot}10)$ (Fig. 1f).

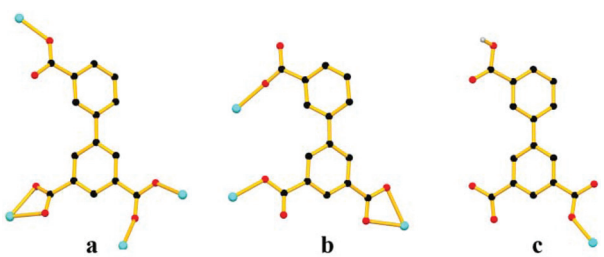

Scheme 2 Coordination modes of ligands in compounds **1–3**.

Crystal structure of $[Mn_3(L)_2(bib)_2(H_2O)_4]{\cdot}4H_2O$ (2)

A single-crystal X-ray diffraction study of compound **2** reveals a 3D architecture that crystallizes in the triclinic system with the $P\bar{1}$ space group. The asymmetric unit consists of one and a half crystallographically independent Mn(II) ions, one completely deprotonated L ligand, one bib ligand, two coordinated water molecules and two water molecules of crystallization. As shown in Fig. 2a, the Mn1 is located in a severely distorted MnN_2O_4 octahedral geometry, completed by one nitrogen atom from one bib ligand [Mn–N = 2.190(2) Å], two oxygen atoms from two coordinated water molecules and three oxygen atoms from two different L ligands [Mn–O = 2.096(7)–2.330(1) Å]. The bond angles around Mn1 range from 56.3(3) to 175.2(3)°. The Mn2 is octahedrally coordinated by two oxygen atoms from two L ligands, two oxygen atoms from two coordinated water molecules [Mn–O = 2.111(8)–2.322(8) Å] and two nitrogen atoms from two bib ligands [Mn–N = 2.243(8) Å], forming a slightly distorted MnN_2O_4 octahedron. O2, O2A, N3 and N3A lie in the apical positions with a bond angle of

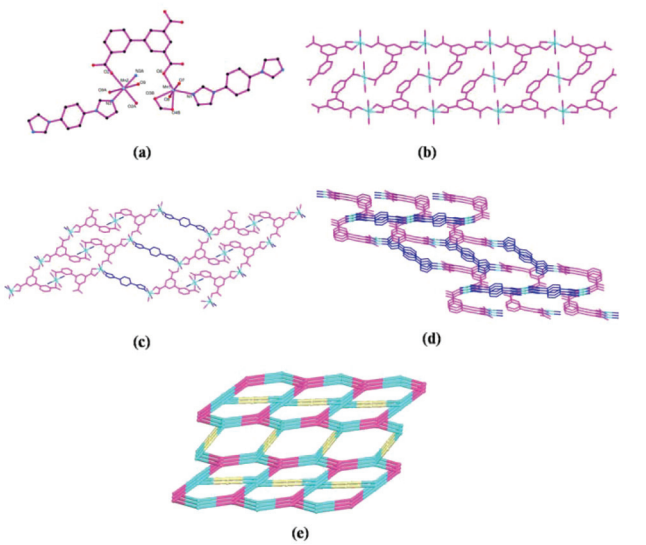

Fig. 2 (a) Coordination environment of Mn(II) in compound **2** (black C, red O, blue N, cyan Mn); (b) the 1D ladder motif of Mn(II) ignoring the connections with bib ligands along the *b* axis; (c) the 2D ladder-like layer of **2** in the *b* plane linked by bib ligands; (d) view of the three-dimensional framework of **2** along the *a* axis; (e) perspective view of the (3,3,4)-connected topology for **2**. Symmetry codes: (A) $-x, 2-y, z$.

180.0(3)°, inducing the difference of the distorted MnN_2O_4 octahedron between Mn1 and Mn2. The bond angles around Mn2 range from 83.8(3) to 180.0(3)°. The ligand of H_3L is completely deprotonated and acts as the μ_3 node to coordinate with three Mn(II) ions, in which three carboxyl groups adopt μ_1–η^1:η^0, μ_1–η^1:η^1 and μ_1–η^0:η^1 coordination modes (Scheme 2b) to form a 1D ladder motif along the *b*-axis (Fig. 2b), which are linked to each other through bib ligands to form a 2D net (Fig. 2c). Moreover, the adjacent nets are further combined through bib ligands with different directions to form a 3D coordination network (Fig. 2d). From the topological point of view, the whole structure of compound **2** can be defined as a (3,3,4)-connected topology with the point symbol of $(6{\cdot}8^2)_2(6^2{\cdot}8)_2(8{\cdot}10^4{\cdot}12)$, while the Mn atoms show 3-connected nodes and L ligands can be simplified as 4-connected nodes, respectively (Fig. 2e).

Crystal structure of [Ni(HL)(bib)(H_2O)$_3$] (3)

The X-ray single-crystal structural analysis shows that compound **3** crystallizes in the orthorhombic system with the $P2_12_12_1$ space group. The asymmetric unit consists of one crystallographically independent Ni(II) ion, one partially deprotonated HL ligand, one coordinated bib ligand and three coordinated water molecules. As depicted in Fig. 3a, the Ni(II) ion is located in a slightly distorted octahedron geometry, which is six-coordinated by two nitrogen atoms from two bib ligands [Ni–N = 2.065(4)–2.066(5) Å], one oxygen atom from one HL ligand and three oxygen atoms from three coordinated water molecules [Ni–O = 2.030(4)–2.106(4) Å]. The Ni(II) ions are bridged by bib ligands to form a 1D left-hand helix chain along the *a*-axis plane, with the pitch of 8.030 Å (Fig. 3b). Ni ions are also coordinated with HL ligands which float outside of the helix chain (Fig. 3c). Interestingly, compound **3** has one partially deprotonated HL ligand and three coordinated water molecules with the former one as the hydrogen-bonding donor and acceptor while the latter one only as the hydrogen-bonding donor. Thus, the adjacent 1D left-handed chains are connected to form the 2D supramolecular layers *via* hydrogen-bonding interactions between oxygen atoms from HL ligands and coordinated water molecules (O3···O6 is 2.661 Å, O6···O8 is 2.709 Å, and O5···O9 is 2.793 Å) (Fig. 3d). Furthermore, the 2D supramolecular layers are interconnected through hydrogen-bonding interactions to generate a 3D supramolecular framework (Fig. 3e) (O9···O2 is 2.999 Å). The H_3L in **3** is partly deprotonated, only exhibiting one kind of coordination mode (Scheme 2c) and acting as a μ_1 node to coordinate with Ni(II) ions to form the 1D left-handed chain.

Crystal structure of [Ni_3(bib)$_4$(H_2O)$_{10}$]·2(L)·12(H_2O) (4)

Single-crystal X-ray diffraction analysis reveals that compound **4** crystallizes in the monoclinic system with the $P2_1/c$ space group. The asymmetric unit of **4** consists of one and a half crystallographically independent Ni(II) ions, two coordinated bib ligands, five coordinated water molecules, one crystallization L ligand and six water molecules of crystallization.

As shown in Fig. 4a, the Ni1 is located in a slightly distorted octahedron geometry, defined by two nitrogen atoms from two bib ligands [Mn–N = 2.190(2) Å] and four oxygen atoms from lattice water molecules. The Ni2 is also octahedrally coordinated by three oxygen atoms from three coordinated water molecules [Mn–O = 2.073(2)–2.352(2) Å] and three nitrogen atoms from three bib ligands [Mn–N = 2.226(3)–2.293(3) Å]. The adjacent Ni(II) ions are connected by bib ligands to form a one-dimensional (1D) ladder motif along the *a* direction (Fig. 4b). Furthermore, the one-dimensional (1D) ladder chain

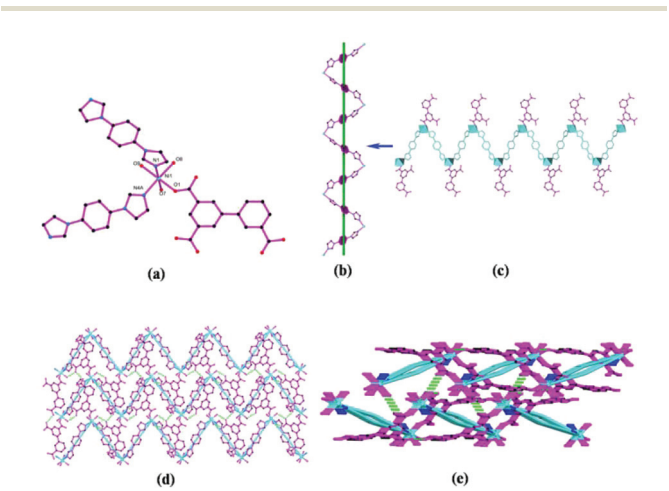

Fig. 3 (a) Coordination environment of Ni(II) in compound **3** (black C, red O, blue N, cyan Ni); (b) the 1D left-hand helix chain along the *a* axis plane connected by bib ligands for **3**; (c) view of the 1D chain coordinated with HL ligands; (d) projection of 2D hydrogen-bonding supramolecular architecture of **3**; (e) view of the 3D supramolecular framework. Symmetry codes: (A) 2.5 − *x*, 1 − *y*, 0.5 + *z*.

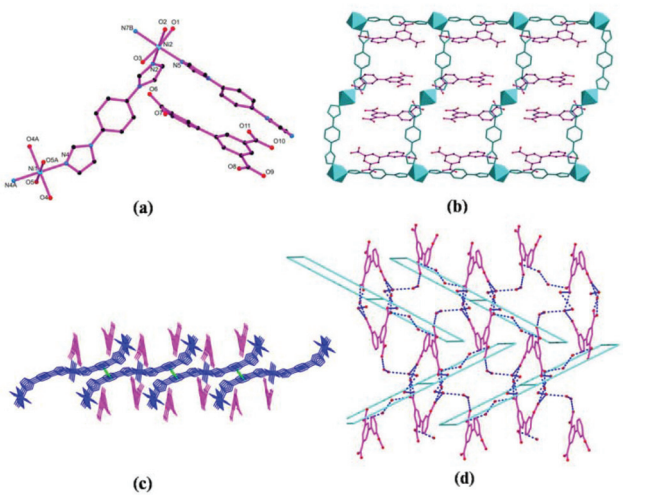

Fig. 4 (a) Coordination environment of Ni(II) in compound **4**; (b) view of the 1D ladder motif along the *a* direction; (c) projection of 2D $\pi\cdots\pi$ stacking supramolecular architecture of **4**; (d) perspective view of the interpenetrating frameworks between the 1D ladder motif and the 2D supramolecular framework. Symmetry codes: (A) −*x*, 1 − *y*, 2 − *z*; (B) −1 + *x*, *y*, *z*.

combined with each other through π···π stacking between the adjacent benzene rings to extend into 2D supramolecular sheets, while the crystallization L ligands are filled in both sides of the 2D supramolecular sheets (Fig. 4c). Differently, although the H_3L in **4** is completely deprotonated, they are not involved in coordination. They exist only in the form of counter ions and hydrogen-bonding acceptors while the three carboxylic groups exhibit μ_0 coordination mode. The hydrogen bonds between L and lattice water, coordinated and uncoordinated water molecules (the hydrogen bond distances and bond angles are listed in Table S3†) linked the adjacent crystallization L ligands to the resulting 2D supramolecular framework which are interdigitated with 1D ladder chains to generate the resulting three-dimensional (3D) supramolecular framework (Fig. 4d).

Effect of the metal ions on the molecular structures

From the structural analysis of **1–4**, we found that compounds **1** and **2** [synthesized by Co(II), Mn(II)] possess high-dimensional architecture while the compounds **3** and **4** [obtained with Ni(II)] have a low-dimensional structure. Taking **1** and **3** as examples, the Co(II) and Ni(II) ions are both six-coordinated and in distorted octahedral geometries; however, their coordination environments are different. In compound **1**, there are two L ligands and three L ligands around each Co1(II) and Co2(II) ion respectively, but in compound **3**, there is only one HL ligand around each Ni(II) ion. Obviously, there are more L ligands around each Co(II) ion than HL ligands around each Ni(II) ion. This is consistent with the fact that the radius of Co(II) ions is larger than that of the Ni(II) ion. Besides, the coordination modes of the H_3L ligands in the two compounds are different (see parts a and c in Scheme 2), which results in different structures of the corresponding compounds. According to the results mentioned above, a rational assembly of metal ions and rigid ligands is critical for the formation of coordination polymers.[13,14]

The effect of solvents used and diverse coordination modes of H_3L

Four new coordination polymers have been successfully synthesized with H_3L and dipyridyl ligands. Compounds **1–3** are taken into account for the same reaction conditions (temperature, pH value and solvent) but for different metal salts, while compounds **3** and **4** are synthesized with the same initial reactants at different solvent ratios. Compound **3** is synthesized with EtOH–H_2O [V(H_2O)–V(EtOH) = 1 : 1]; however, **4** is synthesized in the hydrothermal reaction with EtOH–H_2O [V(H_2O)–V(EtOH) = 3 : 1], which induced different structures between compounds **3** and **4**. It may be attributed to the molecule size of the solvent. H_2O has a smaller van der Waals volume[15] (11.44 cm^3 mol^{-1}), which makes molecules collide more effectively. But the larger van der Waals volume of EtOH (31.94 cm^3 mol^{-1}) makes the system collide with a little difficulty. That is the first reason for the structural difference between **3** and **4**, though the same reactants were mixed initially. Another reason is that the solvent ratio of **4** shows that more water molecules are added to the system, which induces the solubility of organic ligands and makes it difficult for the formation/crystallization of the compound.[16] Contrasting the coordination modes among four CPs, carboxylic ligands show μ_4-bridged mode in **1**, μ_3-bridged mode in **2**, μ_1-bridged mode in **3** and μ_0-bridged mode in **4**. The difference between **1**, **2** and **3** is in the metal salts used, and that between **3** and **4** is in the solvent ratio used. As shown in Scheme 2, the three carboxyl groups of L in **1** adopt μ_1–η^1:η^0, μ_1–η^1:η^1 and μ_2–η^1:η^1 coordination modes to bridge four Co(II) ions to form 2D nets, which can be further linked into a 3D coordination network through the bib ligands. The completely deprotonated carboxyl groups coordinate with three Mn(II) ions with μ_1–η^1:η^0, μ_1–η^1:η^1 and μ_1–η^0:η^1 coordination modes in **2**. It is also worth noting that the three carboxyl groups of L in **2** bridged the adjacent Mn(II) ions to form a 1D ladder motif and further combined through bib ligands to form a 3D coordination network. In compound **3**, only one of the deprotonated carboxyl groups coordinates with Ni(II) ions and adopts μ_1–η^1:η^0 coordination mode, while in **4**, L ligands are completely deprotonated but exhibit μ_0–η^0:η^0 coordination mode. It is obvious that the coordination modes of carboxylic ligands play a crucial role in the construction of novel CPs, which may have a great effect on the dimensions of coordination polymers. We reasonably anticipate that another emergence will occur when new CPs based on the H_3L ligand are further developed and investigated.

X-ray power diffraction analyses and thermal analysis

In order to check the phase purity of **1–4**, the X-ray powder diffraction (PXRD) pattern was checked at room temperature. The experimental and simulated PXRD patterns of **1–4** are shown in Fig. S1–S4†, indicating the phase purity of the products. The differences in intensity may be due to the preferred orientation of the powder samples. To evaluate the thermal stabilities of the four compounds, thermogravimetric analysis (TGA) experiments were performed from 30 to 800 °C (Fig. S5†). For compound **1**, a rapid weight loss was observed from 110 to 220 °C which is attributed to the loss of the coordinated ethanol and the lattice water, with a weight loss of 7.9% (calcd: 8.1%), then the structure was decomposed from 360 °C onwards. The TGA curve of **2** is similar to **1** which lost a great weight of 10.9% (calcd: 11.1%) from 30 to 158 °C due to the loss of the coordinated water and the lattice water, and the framework collapsed at 320 °C. Compound **3** exhibits an initial weight loss of 9.5% (calcd: 9.3%) in the range of 30 to 130 °C, corresponding to the loss of coordinated water and lattice water molecules. Upon further heating, **3** decomposed gradually. For compound **4**, a loss of the lattice water molecules and coordinated water molecules (found: 9.9%, calcd 10.1%) occurs between 105 and 250 °C and the rapid weight loss in the temperature range of 340–400 °C indicates decomposition of the structure. Besides, the bulk sample of **3** was measured using the CD spectrum (Fig. S6†); however, the bulk sample of **3** showed a silent CD spectrum. Therefore, we did not do further research on the chirality of single crystals.

Magnetic properties

The magnetic properties of **1–4** were investigated by solid state magnetic susceptibility measurements in the range 2–300 K with a field of 1000 Oe and are shown in Fig. 5–8. The experimental $\chi_M T$ value of **1** at room temperature is 8.33 cm^3 K mol^{-1}, which is significantly larger than the spin-only value expected for two uncoupled high-spin Co(II) ions (3.75 cm^3 K mol^{-1}). As the sample is cooled, the $\chi_M T$ product shows no significant change from 300 to 125 K and then decreases to a value of 6.74 cm^3 K mol^{-1} at 16 K; below this temperature, a slight rise was observed and then it decreases to a minimum value of 5.99 cm^3 K mol^{-1} at 2 K. Fitting the data of reciprocal susceptibility (χ_M^{-1}) above 20 K to the Curie–Weiss law yielded θ = −3.18 K and C = 8.48 cm^3 K mol^{-1} for **1**. The negative Weiss constant indicates an obvious intra-molecular antiferromagnetic interaction between adjacent Co(II) ions through the carboxyl group. The strengths of the antiferromagnetic exchange interaction and the spin–orbit coupling for Co^{2+} were estimated based on eqn (1).[17]

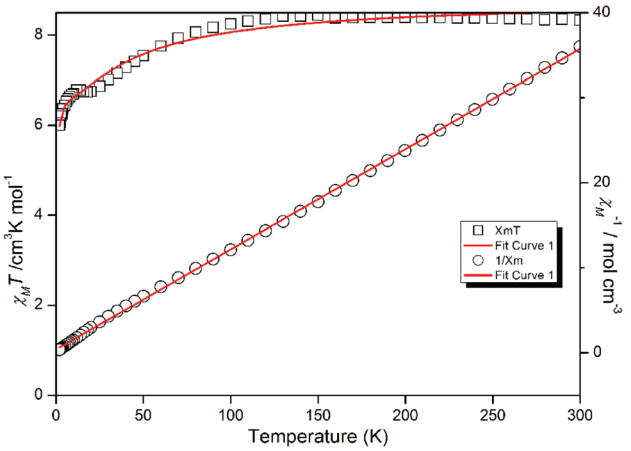

Fig. 5 Temperature dependence of χ_M^{-1} and $\chi_M T$ *vs.* T plot for **1** (open circles and red line represent experimental data and fits).

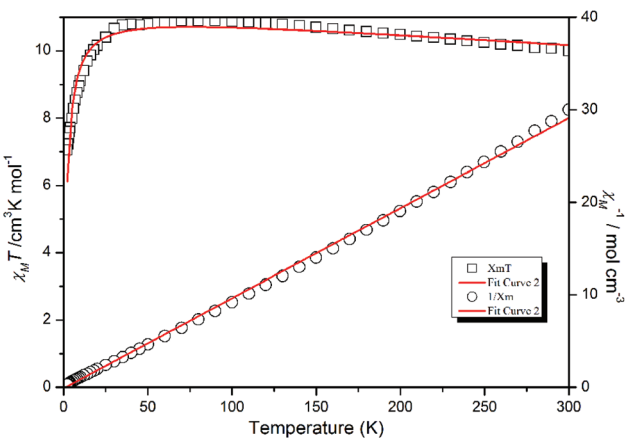

Fig. 6 Temperature dependence of χ_M^{-1} and $\chi_M T$ *vs.* T plot for **2** (open circles and red line represent experimental data and fits).

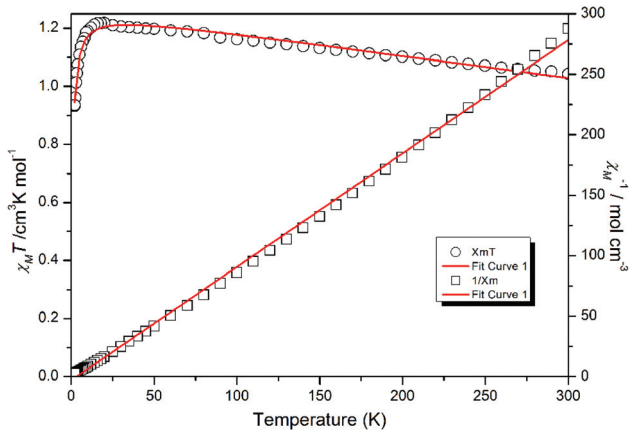

Fig. 7 Temperature dependence of χ_M^{-1} and $\chi_M T$ *vs.* T plot for **3** (open circles and red line represent experimental data and fits).

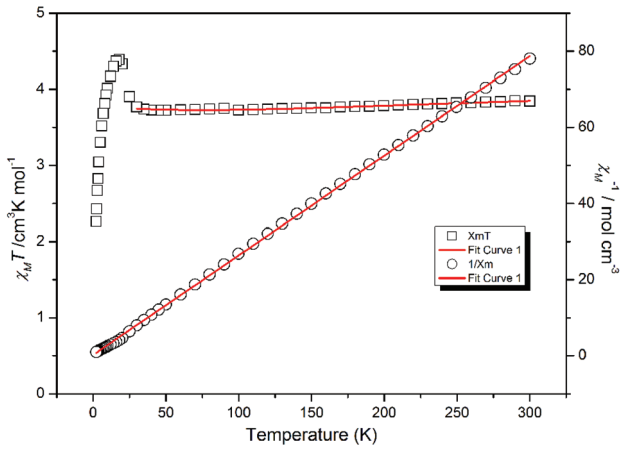

Fig. 8 Temperature dependence of χ_M^{-1} and $\chi_M T$ *vs.* T plot for **4** (open circles and red line represent experimental data and fits).

$$\chi_M T = A \exp(-E_1/kT) + B \exp(-E_2/kT) \quad (1)$$

where $A + B$ equals the Curie constant. The E_1 and E_2 are the spin–orbit coupling constant and the activation energy of antiferromagnetic interactions, respectively. The best fitting gave: E_1/k = 0.24 K, E_2/k = 43.6 K, A = 6.75 cm^3 K mol^{-1}, B = 2.05 cm^3 K mol^{-1} (see Fig. 5). The value for $A + B$ (8.80 cm^3 K mol^{-1}) is consistent with the Curie constant of C = 8.48 according to the Curie–Weiss law.[18] The value for E_1/k is in accordance with those given in the literature for both the effects of spin–orbit coupling and site distortion, and the value $E_2/k \propto -2J$, corresponding to spin coupling between the Co(II) ions, shows the distinct antiferromagnetic exchange mediated between Co(II) through the carboxyl group.

Fig. 6 shows the $\chi_M T$ and χ_M^{-1} *vs.* T plots for compound **2**. When it is cooled from room temperature, the $\chi_M T$ value increases gradually from 9.99 cm^3 K mol^{-1} at 300 K to 10.9 cm^3 K mol^{-1} at 60.0 K, confirming a weak ferromagnetic

exchange between Mn(II) ions. Below this temperature, $\chi_M T$ decreases to a minimum value of 7.05 cm^3 K mol^{-1} at 2 K. The $\chi_M{}^{-1}$ *vs.* T plot obeys the Curie–Weiss law $\chi_M = C/(T - \theta)$ with the Curie constant C = 10.2 cm^3 K mol^{-1} and the Weiss constant θ = 1.19 K. The value of θ further confirms dominant weak ferromagnetic interactions between the Mn(II) ions. From a structural viewpoint, each L ligand coordinated with three Mn(II) ions to form a 1D chain and further extended into 2D nets and 3D frameworks through bib ligands. It should be pointed out that the minimum distance between adjacent 1D ladder motif chains is 13.80 Å so that the bib ligand plays an inappreciable role in propagating magnetic exchanges. This may be attributed to the weak ferromagnetic interactions between the trinuclear units of the 1D ladder motif chain. The interaction between two external Mn(II) ions as well as the trinuclear units can be ignored considering the long distances between them. The magnetic analysis was then carried out using the spin Hamiltonian $\hat{H} = -2J(\hat{S}_1 \cdot \hat{S}_2 + \hat{S}_2 \cdot \hat{S}_3)$, where $\hat{S}_i$ is the spin of the Mn ion number *i*. The eigenvalues are given by eqn (2)

$$E(S_{13}, S) = -J[S(S+1) - S_{13}(S_{13}+1)] \quad (2)$$

$$\chi_M T = \frac{Ng^2\beta^2}{3k} \frac{\sum_{S_{13},S} S(S+1)(2S+1)\exp\left[-\frac{E(S_{13},S)}{kT}\right]}{\sum_{S_{13},S} (2S+1)\exp\left[-\frac{E(S_{13},S)}{kT}\right]} \quad (3)$$

The best fit for compound **2** was obtained for J = 1.82 cm^{-1}, g = 3.21. The agreement factor for $R = \{\sum[(\chi_M)_{obs} - (\chi_M)_{calc}]^2 / \sum[(\chi_M)_{calc}]^2$ is 6.8×10^{-4}. The above features confirm the presence of weak ferromagnetic interactions between the Mn(II) ions in compound **2**.

S is the total spin of the molecule and S_{13} is the spin quantum number associated with the spin $\hat{S}_{13} = \hat{S}_1 + \hat{S}_3$ of the external Mn ions. The resulting magnetic susceptibility is given by the equation below.[19]

For **3**, the $\chi_M T$ and $\chi_M{}^{-1}$ *versus* T plots are shown in Fig. 7. The $\chi_M T$ value of **3** at 300 K is 1.04 cm^3 K mol^{-1}, which is slightly larger than the spin-only value for an isolated S = 1 center (1.0 cm^3 K mol^{-1}). As the temperature decreases, the $\chi_M T$ value increases slightly to a maximum at 17 K of 1.22 cm^3 K mol^{-1}. It only starts to decrease at 17 K reaching a minimum value of 0.93 cm^3 K mol^{-1} at 2 K, which should be mainly attributed to the zero-field splitting of Ni(II) ions. The experimental susceptibility data were fitted to the equation that considers only non-interacting S = 1 ions in the presence of single ion anisotropy. The magnetic susceptibility is given in eqn (4).[20]

$$\chi_M = \frac{2Ng^2\beta^2}{3kT} \times \frac{2x^{-1} - 2\exp(-x)x^{-1} + \exp(-x)}{1 + 2\exp(-x)} \quad (4)$$

where $\chi = J/kT$. The best fit is given by the parameters g = 2.24, J = 2.65 cm^{-1}, and $R = 2.87 \times 10^{-5}$. $R = \{\sum[(\chi_M)_{obs} - (\chi_M)_{calc}]^2 / \sum[(\chi_M)_{calc}]^2$. The J value indicates a weak ferromagnetic exchange within **3**.

As described in Fig. 8, at room temperature, the value of $\chi_M T$ of compound **4** is 3.84 cm^3 K mol^{-1} at 40 K, which is larger than the expected value for spin-only Ni(II) ions. As the temperature is lowered, the $\chi_M T$ value gradually decreases to 3.72 cm^3 K mol^{-1} at 40 K. Upon further cooling, $\chi_M T$ increases dramatically and reaches a maximum of 4.39 cm^3 K mol^{-1} at 18 K. The Curie–Weiss fit of the data above 20 K gives C = 3.81 cm^3 K mol^{-1} and θ = −0.67 K. The negative value of the Weiss constant shows the antiferromagnetic interactions between Ni(II) ions. Below 20 K, the $\chi_M T$ drops quickly and approaches a value of 2.26 cm^3 K mol^{-1} at 2.2 K. The further decrease may be due to the saturation effect.[21] Above 20 K, the strengths of the antiferromagnetic exchange interaction and the spin–orbit coupling for Ni(II) ions were estimated based on eqn (1). (1) $\chi_M T = A\exp(-E_1/kT) + B\exp(-E_2/kT)$, where $A + B$ equals the Curie constant. The best fitting gave: E_1/k = 394.5 K, E_2/k = −0.28 K, A = 0.49 cm^3 K mol^{-1}, B = 3.71 cm^3 K mol^{-1}. The value for $A + B$ (3.82 cm^3 K mol^{-1}) is consistent with the Curie constant of C = 3.81 according to the Curie–Weiss Law. The structural analysis indicates that the distance between the adjacent Ni(II) ions of the 1D ladder-shaped chain is 12.7 Å; such a long distance across the bib ligand plays a negligible role in propagating magnetic exchanges. Because the minimum distance between the adjacent 1D ladder-shaped chains is 3.74 Å, the magnetic exchanges within the adjacent chains are dominant.

Conclusions

In summary, we have successfully synthesized and characterized four new coordination polymers by the self-assembly of the H_3L ligand, the N-donor dipyridyl ligand (bib), and various metal ions under the solvothermal conditions. The structural studies of compounds **1–4** show that coordination modes of carboxylic groups play an important role in the formation of the final structure. Compounds **1**, **2** and **3** show μ_4-carboxylate, μ_3-carboxylate and μ_1-carboxylate bridging modes respectively to meet different coordination requirements of metal ions, and give rise to a distinct structure in the same solvent reaction. Compounds **3** and **4** are synthesized with the same reactants and the structural investigation shows different carboxylate bridges because of the solvent ratio induced. In addition, the magnetic properties of **1–4** have also been investigated, and compounds **1** and **4** show antiferromagnetic interactions between metal ions while compounds **2** and **3** show weak ferromagnetic interactions between metal ions. This research demonstrates that the H_3L ligand can be employed to construct multidimensional coordination polymers exhibiting great structural diversity with various metal ions. Further investigation on the formation of novel coordination polymers based on H_3L with more transition metals is underway in our laboratory.

Acknowledgements

This work was supported by the State Key Program of the National Natural Science of China (no. 20931005), the Key

Research Planning Program of the National Natural Science Foundation of China (grant no. 91022004), the National Natural Science Foundation of China (grant 21371142 and 21201139), the Natural Science Foundation of Shaanxi Province (grant 2013JQ2016), and Science Research Plan Projects of Shaanxi Provincial Educational Department (grant 12JK0605).

Notes and references

1 (*a*) O. M. Yaghi, H. X. Deng, C. J. Doonan, H. Furukawa, R. B. Ferreira, J. Towne, C. B. Knobler and B. Wang, *Science*, 2010, **327**, 846; (*b*) S. B. Choi, H. Furukawa, H. J. Nam, D. Y. Jung, Y. H. Jhon, A. Walton, D. Book, M. O'Keeffe, O. M. Yaghi and J. Kim, *Angew. Chem., Int. Ed.*, 2012, **51**, 8791; (*c*) N. R. Champness, *Chem. Commun.*, 2013, **49**, 331; (*d*) F. Bu, Q. P. Lin, Q. G. Zhai, L. Wang, T. Wu, S. T. Zheng, X. H. Bu and P. Y. Feng, *Angew. Chem., Int. Ed.*, 2012, **51**, 8538; (*e*) X. F. Kuang, X. Y. Wu, R. M. Yu, J. P. Donahue, J. S. Huang and C. Z. Lu, *Nat. Chem.*, 2010, **2**, 461; (*f*) H. Wu, J. Yang, Z. M. Su, S. R. Batten and J. F. Ma, *J. Am. Chem. Soc.*, 2011, **133**, 11406; (*g*) J. Zhang, L. Wojtas, R. W. Larsen, M. Eddaoudi and M. J. Zaworotko, *J. Am. Chem. Soc.*, 2009, **131**, 17040.

2 (*a*) M. O'Keeffe and O. M. Yaghi, *Chem. Rev.*, 2012, **112**, 675; (*b*) B. L. Chen, N. W. Ockwig, A. R. Millward, D. S. Contreras and O. M. Yaghi, *Angew. Chem., Int. Ed.*, 2005, **44**, 4745; (*c*) Y. Cui, Y. Yue, G. Qian and B. L. Chen, *Chem. Rev.*, 2012, **112**, 1126; (*d*) G. Férey and C. Serre, *Chem. Soc. Rev.*, 2009, **38**, 1380; (*e*) L. N. Li, S. Q. Zhang, L. Han, Z. H. Sun, J. H. Luo and M. C. Hong, *Cryst. Growth Des.*, 2013, **13**, 106; (*f*) P. Q. Liao, D. D. Zhou, A. X. Zhu, L. Jiang, R. B. Lin, J. P. Zhang and X. M. Chen, *J. Am. Chem. Soc.*, 2012, **134**, 17380.

3 (*a*) X. L. Zhao, D. Sun, S. Yuan, S. Y. Feng, R. Cao, D. Q. Yuan, S. N. Wang, J. M. Dou and D. F. Sun, *Inorg. Chem.*, 2012, **51**, 10350; (*b*) X. T. Zhang, D. Sun, B. Li, L. M. Fan, B. Li and P. H. Wei, *Cryst. Growth Des.*, 2012, **12**, 3845; (*c*) Q. K. Liu, J. P. Ma and Y. B. Dong, *Chem. Commun.*, 2011, **47**, 12343; (*d*) T. Wen, D. X. Zhang and J. Zhang, *Inorg. Chem.*, 2013, **52**, 12; (*e*) J. P. Zhang, Y. B. Zhang, J. B. Lin and X. M. Chen, *Chem. Rev.*, 2012, **112**, 1001; (*f*) Z. Han, J. Jiang, J. Lu, D. C. Li, S. Cheng and J. M. Dou, *Dalton Trans.*, 2013, **42**, 4777.

4 (*a*) Y. A. Li, S. K. Ren, Q. K. Liu, J. P. Ma, X. Y. Chen, H. M. Zhu and Y. B. Dong, *Inorg. Chem.*, 2012, **51**, 9629; (*b*) S. Yang, X. Lin, A. J. Blake, K. M. Thomas, P. Hubberstey, N. R. Champness and M. Schroöder, *Chem. Commun.*, 2008, 6108; (*c*) J. B. Lin, W. Xue, B. Y. Wang, J. Tao, W. X. Zhang, J. P. Zhang and X. M. Chen, *Inorg. Chem.*, 2012, **51**, 9423; (*d*) C. X. Chen, Q. K. Liu, J. P. Ma and Y. B. Dong, *J. Mater. Chem.*, 2012, **22**, 9027; (*e*) L. Han, L. Qin, L. P. Xu, Y. Zhou, J. L. Sun and X. D. Zou, *Chem. Commun.*, 2013, **49**, 406.

5 (*a*) Y. B. Wang, Y. L. Lei, S. H. Chi and Y. J. Luo, *Dalton Trans.*, 2013, **42**, 1862; (*b*) A. Shigematsu, T. Yamada and H. Kitagawa, *J. Am. Chem. Soc.*, 2011, **133**, 2034; (*c*) D. Sun, L. L. Han, S. Yuan, Y. K. Deng, M. Z. Xu and D. F. Sun, *Cryst. Growth Des.*, 2013, **13**, 377; (*d*) Y. L. Gai, K. C. Xiong, L. Chen, Y. Bu, X. J. Li, F. L. Jiang and M. C. Hong, *Inorg. Chem.*, 2012, **51**, 13128; (*e*) Y. S. Xue, F. Y. Jin, L. Zhou, M. P. Liu, Y. Xu, H. B. Du, M. Fang and X. Z. You, *Cryst. Growth Des.*, 2012, **12**, 6158.

6 (*a*) J. Liu, Y. X. Tan and J. Zhang, *Cryst. Growth Des.*, 2012, **12**, 5164; (*b*) X. Ma, X. Li, Y. E. Cha and L. P. Jin, *Cryst. Growth Des.*, 2012, **12**, 5227; (*c*) H. L. Wang, K. Wang, D. F. Sun, Z. H. Ni and J. Z. Jiang, *CrystEngComm*, 2011, **13**, 279; (*d*) D. P. Zhang, H. L. Wang, L. J. Tian, J. Z. Jiang and Z. H. Ni, *CrystEngComm*, 2009, **11**, 2447; (*e*) J. X. Yang, X. Zhang, J. K. Cheng, J. Zhang and Y. G. Yao, *Cryst. Growth Des.*, 2012, **12**, 333; (*f*) N. L. Torad, M. Hu, Y. Kamachi, K. Takai, M. Imura, M. Naito and Y. Yamauchi, *Chem. Commun.*, 2013, **49**, 2521; (*g*) M. Hu, A. A. Belik, M. Imura and Y. Yamauchi, *J. Am. Chem. Soc.*, 2013, **135**, 384.

7 (*a*) D. Sun, S. Ma, Y. Ke, D. J. Collins and H.-C. Zhou, *J. Am. Chem. Soc.*, 2006, **128**, 3896; (*b*) Z. Guo, H. Wu, G. Srinivas, Y. Zhou, S. Xiang, Z. Chen, Y. Yang, W. Zhou, M. O'Keeffe and B. Chen, *Angew. Chem., Int. Ed.*, 2011, **50**, 3178.

8 (*a*) C. C. Ji, J. Li, Y. Z. Li, Z. J. Guo and H. G. Zheng, *CrystEngComm*, 2011, **13**, 459; (*b*) Z. Y. Guo, H. Xu, S. Q. Su, J. F. Cai, S. Dang, S. C. Xiang, G. D. Qian, H. J. Zhang, M. O'Keeffe and B. L. Chen, *Chem. Commun.*, 2011, **47**, 5551; (*c*) C. S. Lim, J. K. Schnobrich, A. G. Wong-Foy and A. J. Matzger, *Inorg. Chem.*, 2010, **49**, 5271.

9 (*a*) A. G. Wong-Foy, O. Lebel and A. J. Matzger, *J. Am. Chem. Soc.*, 2007, **129**, 15740; (*b*) Z. Y. Guo, G. H. Li, L. Zhou, S. Q. Su, Y. Q. Lei, S. Dang and H. J. Zhang, *Inorg. Chem.*, 2009, **48**, 8069; (*c*) Z. J. Lin, B. Xu, T. F. Liu, M. N. Cao, J. Lü and R. Cao, *Eur. J. Inorg. Chem.*, 2010, **2010**, 3842; (*d*) L. N. Li, J. H. Luo, S. Y. Wang, Z. H. Sun, T. L. Chen and M. C. Hong, *Cryst. Growth Des.*, 2011, **11**, 3744.

10 T. Liu, S. N. Wang, J. Lu, J. M. Dou, M. J. Niu, D. H. Lia and J. F. Bai, *CrystEngComm*, 2013, **15**, 5467.

11 (*a*) G. M. Sheldrick, *SHELXS-97, Program for Crystal Structure Solution*, University of Göttingen, Göttingen, Germany, 1997; (*b*) G. M. Sheldrick, *SHELXL-97, Program for Crystal Structure Refinement*, University of Göttingen, Göttingen, Germany, 1997.

12 V. A. Blatov, M. O'Keeffe and D. M. Proserpio, *CrystEngComm*, 2010, **12**, 44.

13 D. S. Li, J. Zhao, Y. P. Wu, B. Liu, L. Bai, K. Zou and M. Du, *Inorg. Chem.*, 2013, **52**, 8091.

14 D. S. Li, Y. P. Wu, J. Zhao, J. Zhang and J. Y. Lu, *Coord. Chem. Rev.*, 2014, **261**, 1.

15 C. P. Li and M. Du, *Chem. Commun.*, 2011, **47**, 5905.

16 L. Y. Du, W. J. Shi, L. Hou, Y. Y. Wang, Q. Z. Shi and Z. H. Zhu, *Inorg. Chem.*, 2013, **52**, 14018.

17 (*a*) Q. C. Chu, Z. Su, J. Fan, T. A. Okamura, G. C. Lv, G. X. Liu, W. Y. Sun and N. Ueyama, *Cryst. Growth Des.*, 2011, **11**, 3885; (*b*) J. M. Rueff, N. Masciocchi, P. Rabu, A. Sironi and A. Skoulios, *Chem. – Eur. J.*, 2002, **8**, 1813.

18 J. Q. Liu, B. Liu, Y. Y. Wang, P. Liu, G. P. Yang, R. T. Liu, Q. Z. Shi and S. R. Batten, *Inorg. Chem.*, 2010, **49**, 10422.
19 S. Menage, S. E. Vitols, P. Bergerat, E. Codjovi, O. Kahn, J. J. Girerd, M. Guillot, X. Solans and T. Calvet, *Inorg. Chem.*, 1991, **30**, 2666.
20 V. Ramon, E. Albert, S. Xavier and F. B. Mercé, *Inorg. Chim. Acta*, 1996, **248**, 59.
21 (*a*) X.-J. Li, X.-Y. Wang, S. Gao and R. Cao, *Inorg. Chem.*, 2006, **45**, 1508; (*b*) D. K. Rittenberg, K. Sugiura, Y. Sakata, S. Mikami, A. J. Epstein and J. S. Miller, *Adv. Mater.*, 2000, **12**, 126.